

UV and X-ray Spectral Lines of FeXXIII Ion for Plasma Diagnostics

Izumi Murakami and Takako Kato

National Institute for Fusion Science, Nagoya 464-01, Japan

ABSTRACT

We have calculated X-ray and UV spectra of Be-like Fe (FeXXIII) ion in collisional radiative model including all fine-structure transitions among the $2s^2$, $2s2p$, $2p^2$, $2snl$, and $2pnl'$ levels where $n = 3$ and 4, adopting data for the collision strengths by Zhang & Sampson (1992) and by Sampson, Goett, & Clark (1984). Some line intensity ratios can be used for the temperature diagnostics. We show 5 ratios in UV region and 9 ratios in X-ray region as a function of electron temperature and density at $0.3\text{keV} \lesssim T_e \lesssim 10\text{keV}$ and $n_e = 1 - 10^{25}\text{cm}^{-3}$. The effect of cascade in these line ratios and in the level population densities are discussed.

Accepted by *Physica Scripta*

1 Introduction

Intensity ratios of emission lines of ions can be used for plasma diagnostics to investigate physical condition of plasmas. FeXXIII, Be-like Fe ion, is observed in fusion plasma at around $T_e \sim 1\text{keV}$ as well as astrophysical plasmas, such as the solar corona and flares [1], and the intracluster gas [2].

Historically, so-called corona model has been used to calculate level population densities to get intensities of emission lines, considered only collisional excitation from the ground state in the calculation. However, the metastable states play an important role for the population density of L-shell ions even at low density region.

We have constructed collisional radiative model for L-shell ions, including all transitions up to $n = 4$. This model takes into account the effects of excitation from metastable states and radiative cascades from the upper levels.

Bhatia & Mason [3] examined the population densities of FeXXIII, including all transitions among 20 levels, $2s^2$, $2s2p$, $2p^2$, and $2s3l$, and estimated line intensity ratios as a function of electron temperature. Keenan et al. [4] examined the intensity ratios for transitions between $n = 2$ levels of FeXXIII including 10 levels. Since the number of levels considered in their calculations is small, the effect of radiative cascade to the population densities is underestimated.

Here, we calculate the population density of FeXXIII ion by the collisional radiative model, including all transitions among 98 levels of $2s^2$, $2s2p$, $2p^2$, $2snl$, and $2pnl$ ($n \leq 4$) with different data from the previous authors for collision strengths given by Zhang and Sampson [5], and Sampson, Goett, and Clark [6]. Using the results, we study the line intensity ratios as a function of electron temperature and density for plasma diagnostics. We discuss the effect of metastable state and radiative cascade from the upper levels on the population density as well as the line intensity ratio.

2 Atomic Data

The fine structure energy levels and transition probabilities has been calculated by AUTOLSJ method in Dubau et al. [7] by SUPERSTRUCTURE Code for the principal quantum number $n \leq 4$, and 98 levels of the $1s^2 2snl$ and $1s^2 2pnl$ configurations are considered. We have also included a magnetic quadrupole transition probability for $2s^2 \ ^1S_0 - 2s2p \ ^3P_2$ given by Nussbaumer & Storey [8], magnetic dipole transition probabilities for $2s2p(^3P_0 - ^3P_1)$ and for $2s2p(^3P_1 - ^3P_2)$ transitions, and an electric quadrupole transition probability for $2s2p(^3P_0 - ^3P_2)$ transition given by Bhatia and Mason [3].

We have adopted electron collision strengths calculated by Zhang & Sampson [5] for the $\Delta n = 0$ transitions with $n=2$, and those by Sampson, Goett, & Clark [6] for all fine-structure transitions between $n = 2$ and $n = 3$, to get the excitation rate coefficients. We have used modified Mewe's empirical formula [9] for other transitions. For the parameter A of Mewe's Gaunt factor we have adopted $A = 0.075$ which is half of original value for allowed transitions. The excitation rate coefficients calculated by Mewe's empirical formula are checked for available transitions with above data. We have included the proton collisional excitation for the three fine-structure transitions in the $2s2p \ ^3P$ levels, using the cross sections given by Doyle [10].

Zhang & Sampson calculated the collision strengths with relativistic distorted-wave program. Using their data provided as a table, we have calculated the effective collision strength, γ , by approximating the integration with the Maxwellian distribution of electron velocity to a summation used the orthogonal Laguerre polynomials (Formula 25.4.45 in Handbook of Mathematical Functions [11]). Sampson et al. used a relativistic Coulomb-Born-exchange method and gave collision strengths fitted by an analytical form.

The collision strengths used by other authors [3,4] are calculated with different methods. Bhatia & Mason [3] calculated the collision strengths using distorted wave approximation for the transitions between 20 levels. Norrington & Grant [12] used a relativistic

R-matrix code to calculate the collision strengths for transitions among 10 levels, which were used by Keenan et al.[4].

3 Collisional Radiative Model

We have calculated the level population densities and spectrum by Collisional-Radiative Model (CRM). We have taken into account the collisional excitation between all fine-structure transitions including forbidden transitions as well as the radiative transitions;

$$\frac{dn_i}{dt} = - \sum_j (C_{ij}n_e + A_{ij})n_i + \sum_j C_{ji}n_en_i + \sum_{j>i} A_{ji}n_i = 0, \quad (1)$$

where C_{ij} is the excitation rate coefficients from the level i to j , A_{ij} is the radiative transition probability from i to j , n_i is the population density of i level and n_e is the electron density. We assume the equilibrium, $dn_i/dt = 0$, to get the population density, given the electron density and temperature. Here we do not take into account ionization and recombination processes from and/or to other Fe ions. The line intensity per electron and per ion from the level i to j is given as

$$I_{ij}/n_In_e = A_{ij}(n_i/\sum_k n_k)/n_e, \quad (2)$$

where $n_I \equiv \sum n_k$ is to normalize the population density, and n_e is the electron density. We call I_{ij}/n_In_e the effective emission rate coefficient.

3.1 Population Densities

Be-like ions have metastable state of $2s2p\ ^3P_J$ from which the transition probabilities to the ground state, $2s^2\ ^1S_0$, are quite small. Since the probability, $A_r(2s2p\ ^3P_0 - 2s^2\ ^1S_0)$ is zero, the population of the $2s2p\ ^3P_0$ level is not zero even at low density. The reduced population density, $n(i)/g(i)/n(1)$ where $g(i)$ is the statistical weight of the level i , of $2s2p\ ^3P_0$ level is constant, 0.007 for $T_e = 1$ keV, at $n_e \lesssim 10^{12}\text{cm}^{-3}$ and increase above 10^{12}cm^{-3} . At $10^{14} \lesssim n_e \lesssim 10^{16}\text{cm}^{-3}$ the reduced population density of other metastable state, $2s2p\ ^3P_2$, approaches the population density of $2s2p\ ^3P_0$ level and both are nearly

constant. And above 10^{17}cm^{-3} all three metastable levels, $2s2p\ ^3P_{J=0,1,2}$, have almost the same reduced population density. For other levels the population densities increase proportionally to the electron density at $n_e \lesssim 10^{12}\text{cm}^{-3}$. Above 10^{12}cm^{-3} , $2p^2$ levels and some triplet levels of $n = 3$ and 4 have the population densities which vary according to the variation of the population densities of the metastable states. The reduced population densities of all $n = 2$ levels become constant at $n_e \sim 10^{21}\text{cm}^{-3}$ and those of all $n = 3$ and $n = 4$ levels become constant at $n_e \sim 10^{23}\text{cm}^{-3}$, where these levels are to be populated proportionally to the statistical weights [14].

3.2 Emission Line Intensities

Figure 1 shows the effective emission rate coefficients defined by equation (2) for 17 selected transitions as a function of electron temperature at electron density of 10^{11}cm^{-3} , where there is no density effect on line intensities. The transitions are listed in Table 1.

The rate coefficients of transitions among $n = 2$ levels in Figure 1a are monotonic functions of electron temperature, T_e . We find how the cascades affect the line intensities at $T_e \gtrsim 10^7\text{K}$. In Figure 1a, thin lines represent the line intensities calculated with 10 levels, i.e. only $n = 2$ levels (case A) has been made by Keenan et al. [4]. Thick lines are calculated with 46 levels, up to $n = 3$ levels (case B), and the thickest lines are calculated with 96 levels, up to $n = 4$ levels (case C). Each line is labeled with number in Table 1 and A, B, or C indicating case A, B, or C, respectively. The line intensities of case A are almost dominated by the collisional excitation from the ground state and monotonically decrease as electron temperature increases. The differences between thin lines (case A) and thick lines (case B and C) are prominent at $T_e \gtrsim 10^7\text{K}$, which caused by the radiative cascades from the upper levels. In particular, $2p^2$ levels are populated by the cascades considerably and the line intensities increase as the electron temperature increases. For instance, in case A the line intensity of $2s2p\ ^1P - 2p^2\ ^1S$ transition (L_4) is only 10 % of that in case C at $T_e = 10^8\text{K}$ ($\sim 10\text{keV}$). The difference between cases B and C is not so large (1 \sim 14 %) even at $T_e = 10^8\text{K}$. Line intensities at $n_e = 10^{14}\text{cm}^{-3}$

in case C are also plotted with dash-dashed lines labeled as 1' in Figure 1a. L_1 , L_2 , and L_3 are smaller than those at $n_e = 10^{11}\text{cm}^{-3}$ since the population densities divided by n_e for the metastable states are smaller due to collisional excitation from these levels to upper levels. The intensities, L_5 and L_6 , become larger because of the same reason.

Figure 1b shows the effective emission rate coefficients of $n = 3 - 2$ transitions as a function of electron temperature, T_e . In the temperature range of $3 \times 10^6 - 10^8\text{K}$ (0.3keV - 10keV), some intensities increase as temperature increases and some have a maximum. Such different temperature dependences allow us to use line intensity ratios as an indicator of electron temperature. Similarly to $n = 2 - 2$ transitions, the effect of the radiative cascade is seen in the figure. The differences of case B and C become larger at high temperature and are 1% - 28% at $1.2 \times 10^8\text{K}$ (10keV), depending on transitions. $2s3d$ levels are much affected by the cascade.

Figure 1c shows the effective emissions rate coefficients of $n = 4 - 2$ transitions. The temperature dependences are similar to $n = 3 - 2$ transitions. Note that in the calculation of population densities the excitation rate coefficients from $n = 2$ to $n = 4$ transitions are estimated by modified Mewe's formula mentioned in Sec.2.

4 Line Intensity Ratios

We have chosen 17 strong lines to measure the electron temperature of a plasma, which are summarized in Table 1. Five ratios from six lines chosen among $n = 2 - 2$ transitions in UV spectrum, are taken to be examined, as selected by Keenan et al. [4]. Six ratios from seven lines chosen among $n = 3 - 2$ transitions at around 11 Å in X-ray spectrum, and three ratios from four lines chosen among $n = 4 - 2$ transitions at around 8 Å are considered. We summarize the line ratios in Table 2.

4.1 Density Dependences

First, we investigate the density dependence of the above line ratios. Figure 2 shows the line ratios listed in Table 2 as a function of electron density, n_e , at electron temperature of $1.2 \times 10^7 \text{K}$ (1keV). There is no density dependence seen at $n_e \lesssim 10^{12} \text{cm}^{-3}$. R_6 and R_{12} are relatively insensitive to the density in the whole range, while R_2 , R_3 , R_5 , R_9 , and R_{10} vary above $n_e \gtrsim 10^{12} \text{cm}^{-3}$. Their density dependences are caused by the variation of population densities of metastable levels. The variation of R_5 at $10^{12} \lesssim n_e \lesssim 10^{16} \text{cm}^{-3}$ is caused by the population density of $2s2p \ ^3P_2$ level. The population density becomes nearly constant and the effective emission rate coefficient of the line, L_3 , decreases proportionally to the electron density (see eq.(2)). Meanwhile the population density of $2s3p \ ^3P_1$ level increases proportionally to the electron density and the effective emission rate coefficient of L_2 keeps constant. At this density region, the variation of the population densities of $2s2p \ ^3P_{J=0,2}$ levels affects the population densities of $2p^2 \ ^3P_2$ and 1D levels, and then the line ratios, R_2 and R_3 , vary. The variation of $R_1 - R_4$ at $10^{17} \lesssim n_e \lesssim 10^{21} \text{cm}^{-3}$ is caused by the decrease of the effective emission rate coefficient of L_2 line, because the population density of $2s2p \ ^3P_1$ level increases slower than the increase of the electron density. Other ratios are almost constant at $n_e \lesssim 10^{16} \text{cm}^{-3}$.

For tokamak plasmas at electron density around $10^{13} - 10^{14} \text{cm}^{-3}$ the line ratios, R_2 , R_4 , R_5 , R_9 , and R_{10} , are not good for temperature diagnostic because of strong density dependences. Checked the temperature dependences of these ratios in next section, the ratio R_5 is found to be quite good for density diagnostic because of the small temperature dependence. Other ratios have possibilities to be used for temperature diagnostic.

4.2 Temperature Dependences

Figure 3 shows the line intensity ratios as a function of electron temperature at $n_e = 10^{11} \text{cm}^{-3}$. For R_1 to R_5 , we plot calculated ratios, including 10 levels (case A), with 46 levels (case B), and with 98 levels (case C), together with the ratios obtained by

Keenan et al. [4]. For R_6 to R_{10} , ratios in cases C and B are plotted. Crosses in Figures 3(e)-(h) are ratios estimated from results by Bhatia and Mason [3] at an electron density of 10^9cm^{-3} . There is no density dependence for these line ratios at this density range. Bhatia and Mason obtained these ratios with 20 levels. When we calculated the ratios with the same 20 levels, such line ratios are different by 1 % or less from the ratios calculated in case B (46 levels) in which $2pnl$ levels are included. So we can compare their ratios with ours in case B. Those ratios at $n_e = 10^{14}\text{cm}^{-3}$ in case C are also plotted in the figure.

Comparing $R_1 - R_5$ in case A with the ratios obtained by Keenan et al., we find that the differences are 1 % - 33 % and tend to increase as temperature increases. The ratios, R_3 and R_4 , are much different from Keenan et al.'s results. The difference is caused by the different excitation cross sections from the ground state to $2p^2$ states.

When we include $n = 3$ and 4 levels in the calculations, the line ratios are significantly changed, especially at higher temperatures. It is because of the influence of the cascades from the upper levels contributing to the population densities and line intensities, as seen from Figure 1a. For example, R_2 in case C is 93 % of R_2 in case A at $T_e = 3.5 \times 10^6\text{K}$ (0.3keV), 57 % at $T_e = 1.2 \times 10^7\text{K}$ (1keV), and 32 % at $T_e = 1.2 \times 10^8\text{K}$ (10keV). Similarly to the line intensities themselves, the intensity ratios are much affected by the cascade. Because the population densities of the metastable states depend on the density at $n_e \lesssim 10^{12}\text{cm}^{-3}$ and the collisional excitation from the metastable states starts to affect the population densities of upper levels, R_2 , R_3 , and R_5 show different temperature dependences at $n_e = 10^{14}\text{cm}^{-3}$.

As seen in Figures 3(e)-(h), the ratios, R_6-R_{10} , are mostly different from those obtained by Bhatia and Mason. R_7 shows good agreement with that of Bhatia and Mason within 10 % difference. In particular, R_6 and R_8 in case B are different by 17-48 % from Bhatia and Mason. Those differences are caused by difference of the excitation cross section. The collision strength of $2s^2\ ^1S - 2s3d\ ^1D$ obtained by Sampson et al. increases

monotonically as the incident electron energy increases, while that of Bhatia and Mason decreases at higher energy. In addition the collision strength of Sampson et al. is always larger than that of Bhatia and Mason. These two effects increase the population density of $2s3d\ ^1D$, resulting in different value for R_6 between Bhatia and Mason and ours. For R_8 , the collision strengths of $2s^2\ ^1S - 2s3p\ ^1P$ and $2s^2\ ^1S - 2s3p\ ^3P_1$ obtained by Sampson et al. increase similarly according to the increase of the incident electron energy, while the collision strength of $2s^2\ ^1S - 2s3p\ ^1P$ obtained by Bhatia and Mason increases faster than that of $2s^2\ ^1S - 2s3p\ ^3P$. This causes the different temperature dependences for R_8 . The ratios of R_9 and R_{10} decrease slower than those of Bhatia and Mason at higher temperature.

The effect on the line ratios by including $n = 4$ levels is small, by amount up to 25 %, for all ratios considered here. We may note that it is important to include levels up to $n = 3$ at least in calculations with CRM to get reliable line intensity ratios for temperature diagnostics.

As R_8 and R_{11} show poor temperature dependence, a combined usage of these ratios with others is quite helpful to check the calibration of spectrometer. R_9 and R_{10} depend slightly on electron density. R_9 at 10^{14}cm^{-3} is 1.6-2.4 times larger than that at 10^{11}cm^{-3} , and R_{10} at 10^{14}cm^{-3} is 1.2 times larger that at 10^{11}cm^{-3} .

Although the line intensities of $n = 4 - 2$ transitions are weak, the wavelength region is not so crowded and these lines is expected to be useful for plasma diagnostics because of being unblended. R_{12} is sensitive to electron temperature similarly to R_{11} , while R_{13} is quite insensitive to temperature.

5 Discussion

5.1 Contribution of Cascade and Metastable State

We have found that the cascades are important for dominating an emission line intensity. The effect of the cascade can be examined with population densities which are analyti-

cally calculated with following equation (3) . Only collisional excitation from the ground state and radiative transitions are considered in the equation. Neglected transitions are unimportant at $n_e \lesssim 10^{15} \text{cm}^{-3}$.

$$\frac{n_i}{n_1} = \frac{C_{1i}n_e}{\sum_{j=1}^{i-1} A_{ij}} + \sum_{k=i+1}^m \frac{n_k}{n_1} \frac{A_{ki}}{\sum_{j=1}^{i-1} A_{ij}}, \quad (3)$$

where level 1 means the lowest level and level m means the highest level, which is 98 in this case. The first term in the right hand side is the contribution of the collisional excitation from the ground state and the second term represents the contribution of the cascades. This equation can be calculated from the highest level for descending k . Similarly, we can also examine the effect of the metastable state to the population densities separately, changing the lowest level in equation (3) to be the metastable state, $2s2p \ ^3P_0$.

Comparing the population densities obtained with equation (3) and those by CRM with equation (1), we find that the cascade from $n = 3$ to $n = 2$ levels are important to the population densities of $n = 2$ levels, especially $2p^2$ state. For example, Figure 4 shows each contribution of the collisional excitation from the ground state (white in the figure), of the cascade (vertical-striped, from $n=4$ levels; dotted, from $n=3$ levels; lateral-striped, from $n=2$ levels), and of the metastable state (black), to population density for each level in the plasma at $n_e = 10^{11} \text{cm}^{-3}$ and $T_e = 1.2 \times 10^7 \text{K}$ (1keV). Sixty % of the population density of $2p^2 \ ^1S_0$ level and 17 % of that of $2s2p \ ^3P_1$ level are fed by the cascade. Cascade from $n = 4$ to $n = 2$ levels contributes the population densities by 1-10 % to $n = 2$ levels and is also effective for $2p3l$ levels and $2s3l$ triplet levels. Such percentages depend on the electron density and temperature. The results are consistent with the arguments on the differences of line intensities in cases A, B, or C, which include different number of levels in the model (§3.2).

The contribution originated from the metastable state to the population densities is mostly small, however, some triplets and $2p3l$ levels, such as $2p^2 \ ^3P_1$, $2p3s \ ^3P_0$, $2p3p \ ^1P$, and $2p3d \ ^3D_2$, have more than 50 % contribution from the metastable state. The

contributions of the metastable state to L_2 , L_3 , L_5 , L_6 , L_{11} , and L_{12} line intensities are 6%, 10%, 6%, 4%, 2%, and 2%, respectively, at $n_e = 10^{11}\text{cm}^{-3}$ and $T_e = 1.2 \times 10^7\text{K}$ (1keV). The contributions to other lines are much less than 1%. At higher densities, the collisional excitation from excited states cannot be neglected and the equation (3) should not be used.

5.2 Comparison with Observations of the Solar Flares

There are some observations of FeXXIII lines in the Sun. Mason et al. (1984) [14] observed a solar flare with *OSO 5* satellite and measured the intensity ratio, R_1 , from the spectrum. They obtained $R_1 \simeq 23$ with $\sim 25\%$ uncertainty. Keenan et al. discussed that their theoretical result was in good agreement with the observation of Mason et al. Our ratio, R_1 , in case C is different by 4-10 % from the ratio of Keenan et al., however, it still agrees with the observation within the uncertainty, at the temperature where Be-like Fe (FeXXIII) ion has the maximum fractional abundance in ionization equilibrium ($T_e = 10^{7.1}\text{K}$ ($\sim 1\text{keV}$); Arnaud & Rothenflug 1985 [15]). Our ratio gives a larger temperature than the ratio of Keenan et al. did. Because of the measurement error it is not possible to determine the electron temperature of the solar flare in this case.

McKenzie et al. (1985) [1] observed a solar flare with *SOLEX* and showed the emission lines in the 5.5 - 12 Å range. They detected 4 lines of $n = 3 - 2$ transitions and 2 lines of $n = 4 - 2$ transitions. Since the lines at ~ 11 Å are blended and the background level is not easy to determine, their line intensities have a large uncertainty. The ratio, R_6 , is measured as 2.04 by McKenzie et al. The authors concluded that the ratio was in good agreement with one estimated by Bhatia and Mason. In our case, this ratio indicates $T_e \sim 10^{7.6 \pm 0.3}\text{K}$, which is higher than the temperature, $10^{7.1 \pm 0.2}\text{K}$, given by the ratio of Bhatia and Mason. On the other hand, the ratio, R_{12} , from $n = 4 - 2$ transitions is measured as 0.89 by McKenzie et al., and this indicates $T_e \sim 10^{7.1}\text{K}$.

In future *SOHO* satellite will observe solar FeXXIII lines and will provide us more

observational data to be compared with theoretical calculations.

6 Concluding Remarks

We study the spectrum of Be-like Fe (FeXXIII) ion for plasma diagnostic and show some useful pairs of the emission lines for temperature diagnostic. In the collisional-radiative model we have included all fine structure levels up to $n = 4$ (98 levels). This is new work because previous work for plasma diagnostics includes levels of up to $2s3l$ (20 levels) [3]. We find the importance of the cascade from upper levels to the population density. However, in this study we do not take into account the effects of ionization and recombination to/from other ions.

Radiative and dielectronic recombination from Li-like Fe (FeXXIV) ion will contribute much to population densities as like radiative cascade, especially at low temperature. For example, total dielectronic recombination rate coefficient is about $7 \times 10^{-12} \text{cm}^3 \text{s}^{-1}$ at $T_e = 1.2 \times 10^7 \text{K}$ (1keV) (Moribayashi et al. 1995 [16]) and the process will affect weak lines such as L_4-L_6 , $L_{10}-L_{17}$. The recombination will increase the line intensity of L_2 , $2s^2 \ ^1S - 2s2p \ ^3P_1$, by 13 % at the maximum when ion abundances of Li-like (FeXXIV) and Be-like (FeXXIII) ions are assumed to be equal.

Inner-sub shell ionization, $2s^2 2p + e \rightarrow 2s2p + 2e$, from B-like Fe (FeXXII) will make the population density of metastable state increase, which will affect the densities of other levels (Kato et al. 1995 [17]). The inner-sub shell ionization rate coefficient can be estimated as $6.3 \times 10^{-12} \text{cm}^3 \text{s}^{-1}$ at $1.2 \times 10^7 \text{K}$ (1keV) with Lotz's formula [18]. If the rate coefficient to $2s2p \ ^3P_0$ level is estimated with the above value weighted with the statistical weight, the population density of the level would increase by 25% with this process, compared with the excitation rate coefficient from the ground state. Here we assume that ion abundances of B-like (FeXXII) and Be-like (FeXXIII) ions are equal. The contribution of the line intensity of L_2 will be 3%. At higher temperature or with the suprathreshold electrons the contribution will increase and the process will be more

important. Therefore we need to include such effects to the calculation in the future work.

Acknowledgments

We acknowledge H.L.Zhang for providing us his data of the collision strengths for $n=2 - n = 2$ transitions.

References

- [1] McKenzie, D.L., Landecker, P.B., Feldman, U., and Doschek, G.A., *Astrophys.J.*, **289**, 849 (1985)
- [2] Fabian, A.C., Arnaud, K.A., Bautz, M.W., and Tawara, Y., *Astrophys.J.*, **436**, L63 (1994)
- [3] Bhatia, A.K. and Mason, H.E., *Astron. Astrophys.*, **103**, 324 (1981)
- [4] Keenan, F.P., Conlon, E.S., Warren, G.A., Boone, A.W., and Norrington, P.H., *Astrophys.J.*, **405**, 350 (1993)
- [5] Zhang, H.L. and Sampson, D.H., *Atomic Data and Nuclear Data Tables*, **52**, 143 (1992)
- [6] Sampson, D.H., Goett, S.J., and Clark, R.E.H., *Atomic Data and Nuclear Data Tables*, **30**, 125, (1984)
- [7] Dubau, J., Cornille, M., Bely-Dubau, F., Faucher, P., and Kato, T., “New Horizon of X-ray Astronomy - First Results from ASCA, *Frontiers Science Series No. 12* ” (Universal Academy Press, Tokyo), 615 (1994)
- [8] Nussbaumer, H. and Storey, P.J., *J. Phys. B.*, **12**, 1647, (1979)
- [9] Mewe, R., *Astron. Astrophys.*, **20**, 215 (1972)
- [10] Doyle, J.G., *Atomic Data and Nuclear Data Tables*, **37**, 441 (1987)
- [11] *HandBook of Mathematical Functions* ed. M. Abramowitz and I. A. Stegun (New York, Dover), p.890 (1965).
- [12] Norrington, P.H. and Grant, I.P., *J. Phys. B*, **20**, 4869 (1987)

- [13] Murakami, I., Kato, T., and Dubau, J., Research Report of the National Institute for Fusion Science, NIFS-DATA-35 (1996)
- [14] Mason, H.E., Bhatia, A.K., Kastner, S.O., Neupert, W.M., & Swartz, M., Sol. Phys., **92**, 199 (1984)
- [15] Arnaud, M. & Rothenflug, R., Astron. Astrophys. Suppl. **60**, 425 (1985)
- [16] Moribayashi, K., Kato, T., & Safronova, U., submitted to Fusion Engineering and Design (1995)
- [17] Kato, T. et al. submitted to Fusion Engineering and Design (1995)
- [18] Lotz, W., Astrophys.J.Suppl., **14**, 207 (1967)

Figure Captions

Fig. 1. Effective emission rate coefficients as a function of electron temperature at an electron density of 10^{11}cm^{-3} . Horizontal axis is for the electron temperature measure in K (lower axis) or keV (upper axis). (a) Coefficients for transitions among $n = 2$ levels. The heaviest lines are calculated in case C including 98 levels up to $n = 4$, heavy lines are in case B including 46 levels up to $n = 3$, and thinnest lines are in case A including 10 levels of $n = 2$. Each line is labeled with numbers in Table 1 and A, B, or C for cases A, B, or C, respectively. 1A means L_1 lines in case A, and so on. Long dash-short dashed lines labeled with number with prime such as 1' are in case C at an electron density of 10^{14}cm^{-3} . The line 4' is overlapped with the line 4C at $n = 10^{11}\text{cm}^{-3}$; (b) For transitions from $n = 3$ to $n = 2$ levels. Heavy lines are calculated in case C and thin lines are in case B. Similar to Fig.1a, each line is labeled with number in Table 1 ; and (c) For transitions from $n = 4$ to $n = 2$ levels. Similar to Fig.1a, each line is labeled with number in Table 1.

Fig. 2. The theoretical FeXXIII emission-line ratios as a function of electron density at electron temperature of $T_e = 1$ keV. Fourteen ratios from R_1 to R_{14} listed in Table 2 are plotted.

Fig. 3. The theoretical FeXXIII emission-line ratios as a function of electron temperature at an electron density of $n_e = 10^{11}\text{cm}^{-3}$. Ratios are listed in Table 2. The label A indicates ratio calculated in case A including 10 levels of $n = 2$, B indicates case B including 46 levels up to $n = 3$, and C indicates case C including 98 levels up to $n = 4$. Ratios at $n_e = 10^{14}\text{cm}^{-3}$ in case C are also plotted with dotted lines, some of which are overlapped with lines in case C at $n = 10^{11}\text{cm}^{-3}$. Lines labeled with K in panels (a)-(d) are results by Keenan et al.[4] and crosses in panels (e)-(h) are results by Bhatia and Mason [3].

Fig. 4. The fraction of each contribution to population density of each level at $n \leq 3$, at $T_e = 1\text{keV}$ and $n_e = 10^{11}\text{cm}^{-3}$. White shows the contribution of the collisional excitation from the ground state. The contributions of cascade from $n = 2$ levels, $n = 3$ levels, and $n = 4$ levels, are shown by lateral-striped, dotted, and vertical-striped, respectively. Black shows the contribution of both collisional excitation and cascade originated from the metastable state, $2s2p\ ^3P_0$.

Table 1: Strong Emission Lines of FeXXIII Ions

label	transitions	wavelength (in Å)	(in eV) [7]
L_1	$\dots 2s^2 \ ^1S - 2s2p \ ^1P$	131.48 Å	94.296eV
L_2	$\dots 2s^2 \ ^1S - 2s2p \ ^3P_1$	267.62 Å	46.328eV
L_3	$\dots 2s2p \ ^3P_1 - 2s2p \ ^3P_2$	976.78 Å	12.693eV
L_4	$\dots 2s2p \ ^1P - 2p^2 \ ^1S$	146.21 Å	84.800eV
L_5	$\dots 2s2p \ ^1P - 2p^2 \ ^1D$	219.43 Å	56.502eV
L_6	$\dots 2s2p \ ^3P_2 - 2p^2 \ ^3P_2$	167.33 Å	74.097eV
L_7	$\dots 2s2p \ ^1P - 2s3d \ ^1D$	11.725 Å	1057.4 eV
L_8	$\dots 2s2p \ ^1P - 2s3s \ ^1S$	12.149 Å	1020.5 eV
L_9	$\dots 2s^2 \ ^1S - 2s3p \ ^1P$	10.966 Å	1130.7 eV
L_{10}	$\dots 2s^2 \ ^1S - 2s3p \ ^3P_1$	11.006 Å	1126.5 eV
L_{11}	$\dots 2s2p \ ^3P_2 - 2s3d \ ^3D_3$	11.429 Å	1084.8 eV
L_{12}	$\dots 2s2p \ ^3P_1 - 2s3d \ ^3D_2$	11.308 Å	1130.8 eV
L_{13}	$\dots 2p^2 \ ^1S - 2p3d \ ^1P$	11.869 Å	1044.6 eV
L_{14}	$\dots 2s2p \ ^1P - 2s4d \ ^1D$	8.8074 Å	1407.7 eV
L_{15}	$\dots 2s^2 \ ^1S - 2s4p \ ^1P$	8.2934 Å	1495.0 eV
L_{16}	$\dots 2s2p \ ^1P - 2s4s \ ^1S$	8.8998 Å	1393.1 eV
L_{17}	$\dots 2s^2 \ ^1S - 2s4p \ ^3P_1$	8.3059 Å	1492.7 eV

Table 2: Emission Lines Ratios for Plasma Diagnostics

label	ratios	with labels in Table 1
R_1	$\dots I(2s^2\ ^1S - 2s2p\ ^1P)/I(2s^2\ ^1S - 2s2p\ ^3P_1)$	L_1/L_2
R_2	$\dots I(2s^2\ ^1S - 2s2p\ ^3P_1)/I(2s2p\ ^3P_2 - 2p^2\ ^3P_2)$	L_2/L_6
R_3	$\dots I(2s^2\ ^1S - 2s2p\ ^3P_1)/I(2s2p\ ^1P - 2p^2\ ^1D)$	L_2/L_5
R_4	$\dots I(2s^2\ ^1S - 2s2p\ ^3P_1)/I(2s2p\ ^1P - 2p^2\ ^1S)$	L_2/L_4
R_5	$\dots I(2s^2\ ^1S - 2s2p\ ^3P_1)/I(2s2p\ ^3P_1 - 2s2p\ ^3P_2)$	L_2/L_3
R_6	$\dots I(2s2p\ ^1P - 2s3d\ ^1D)/I(2s^2\ ^1S - 2s3p\ ^1P)$	L_7/L_9
R_7	$\dots I(2s^2\ ^1S - 2s3p\ ^1P)/I(2s2p\ ^1P - 2s3s\ ^1S)$	L_9/L_8
R_8	$\dots I(2s^2\ ^1S - 2s3p\ ^3P_1)/I(2s^2\ ^1S - 2s3p\ ^1P)$	L_{10}/L_9
R_9	$\dots I(2s2p\ ^3P_2 - 2s3d\ ^3D_3)/I(2s^2\ ^1S - 2s3p\ ^1P)$	L_{11}/L_9
R_{10}	$\dots I(2s2p\ ^3P_1 - 2s3d\ ^3D_2)/I(2s^2\ ^1S - 2s3p\ ^1P)$	L_{12}/L_9
R_{11}	$\dots I(2p^2\ ^1S - 2p3d\ ^1P)/I(2s^2\ ^1S - 2s3p\ ^1P)$	L_{13}/L_9
R_{12}	$\dots I(2s^2\ ^1S - 2s4p\ ^1P)/I(2s2p\ ^1P - 2s4d\ ^1D)$	L_{14}/L_{13}
R_{13}	$\dots I(2s2p\ ^1P - 2s4s\ ^1S)/I(2s2p\ ^1P - 2s4d\ ^1D)$	L_{15}/L_{13}
R_{14}	$\dots I(2s^2\ ^1S - 2s4p\ ^3P_1)/I(2s2p\ ^1P - 2s4d\ ^1D)$	L_{16}/L_{13}

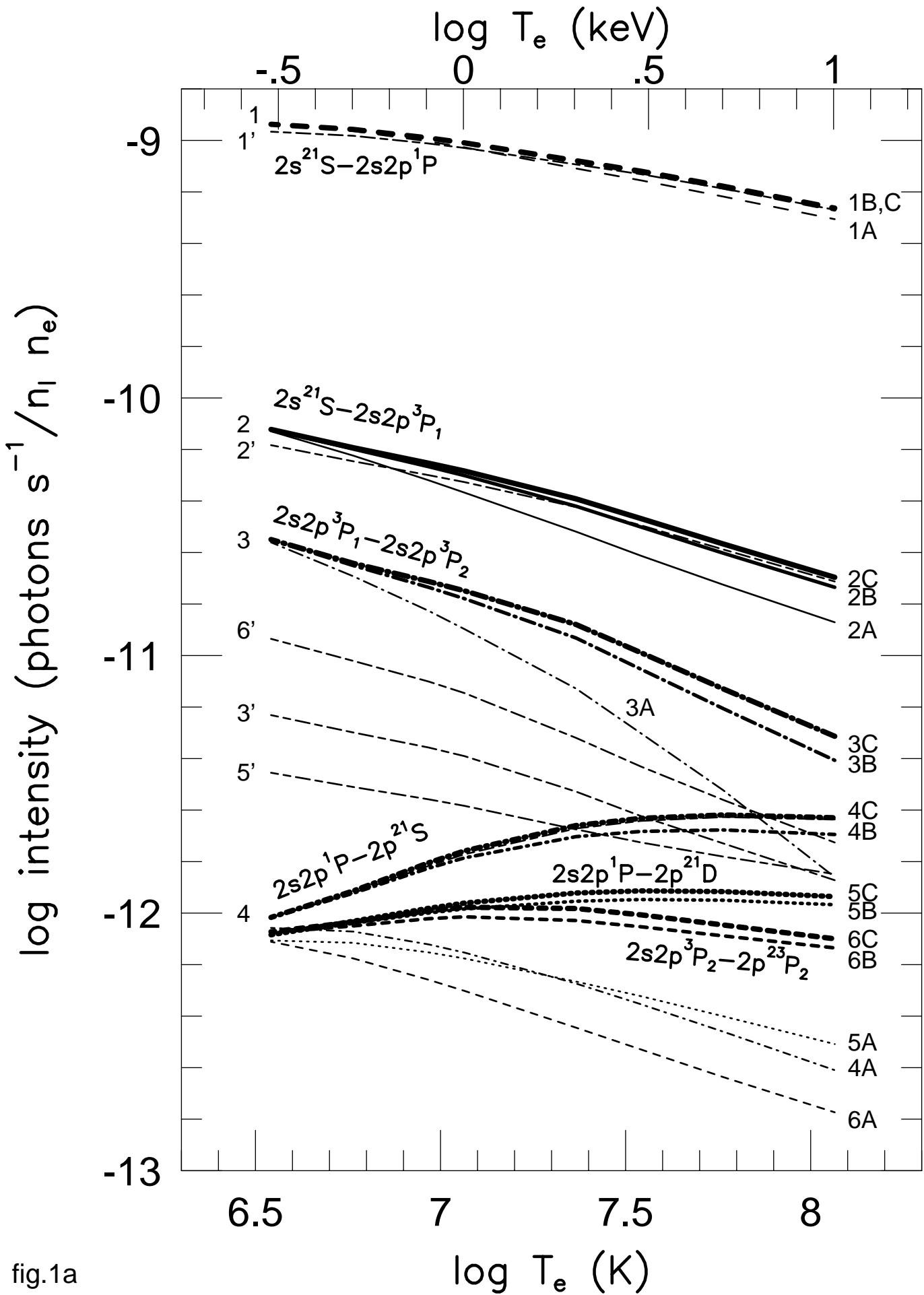


fig.1a

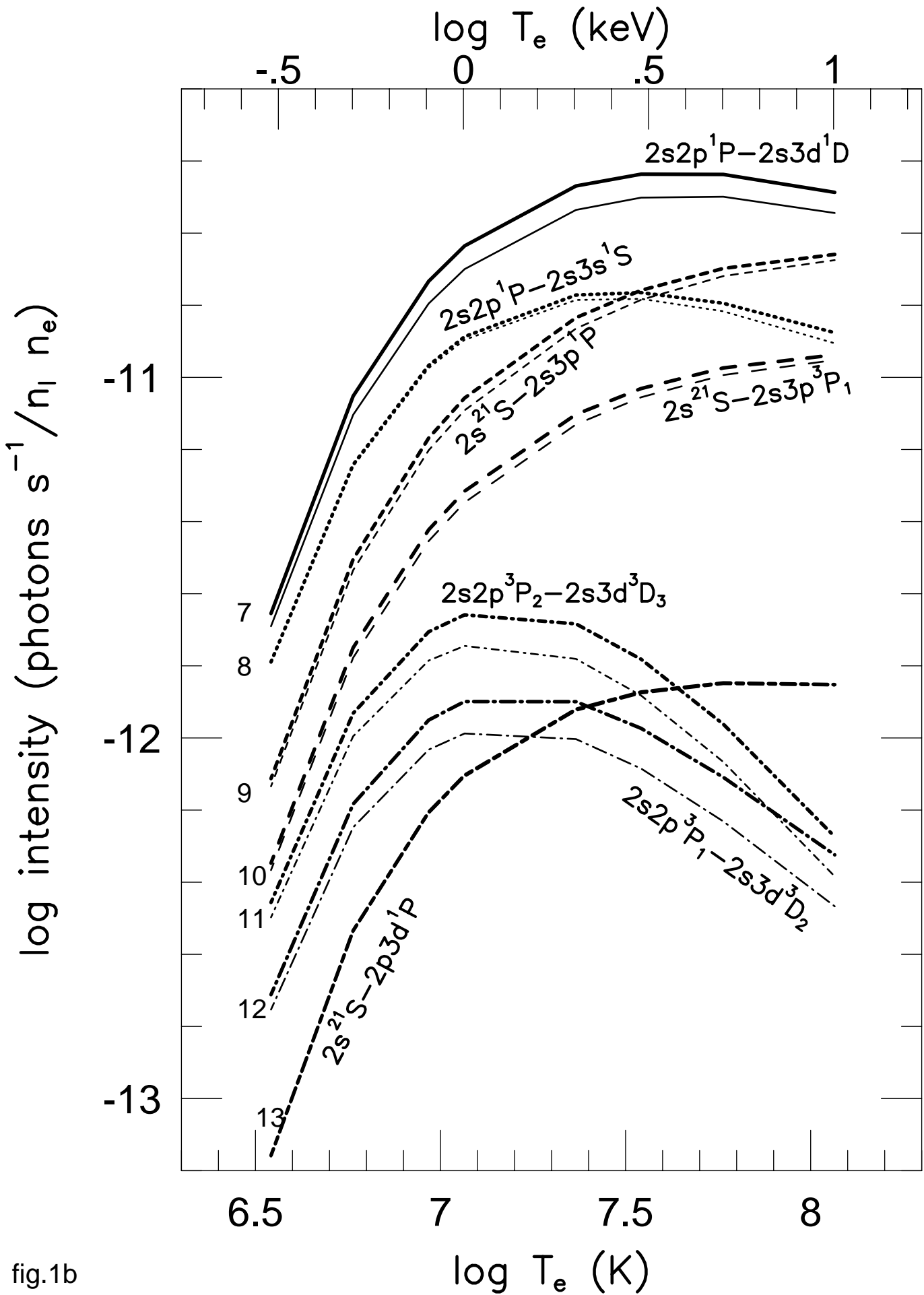


fig.1b

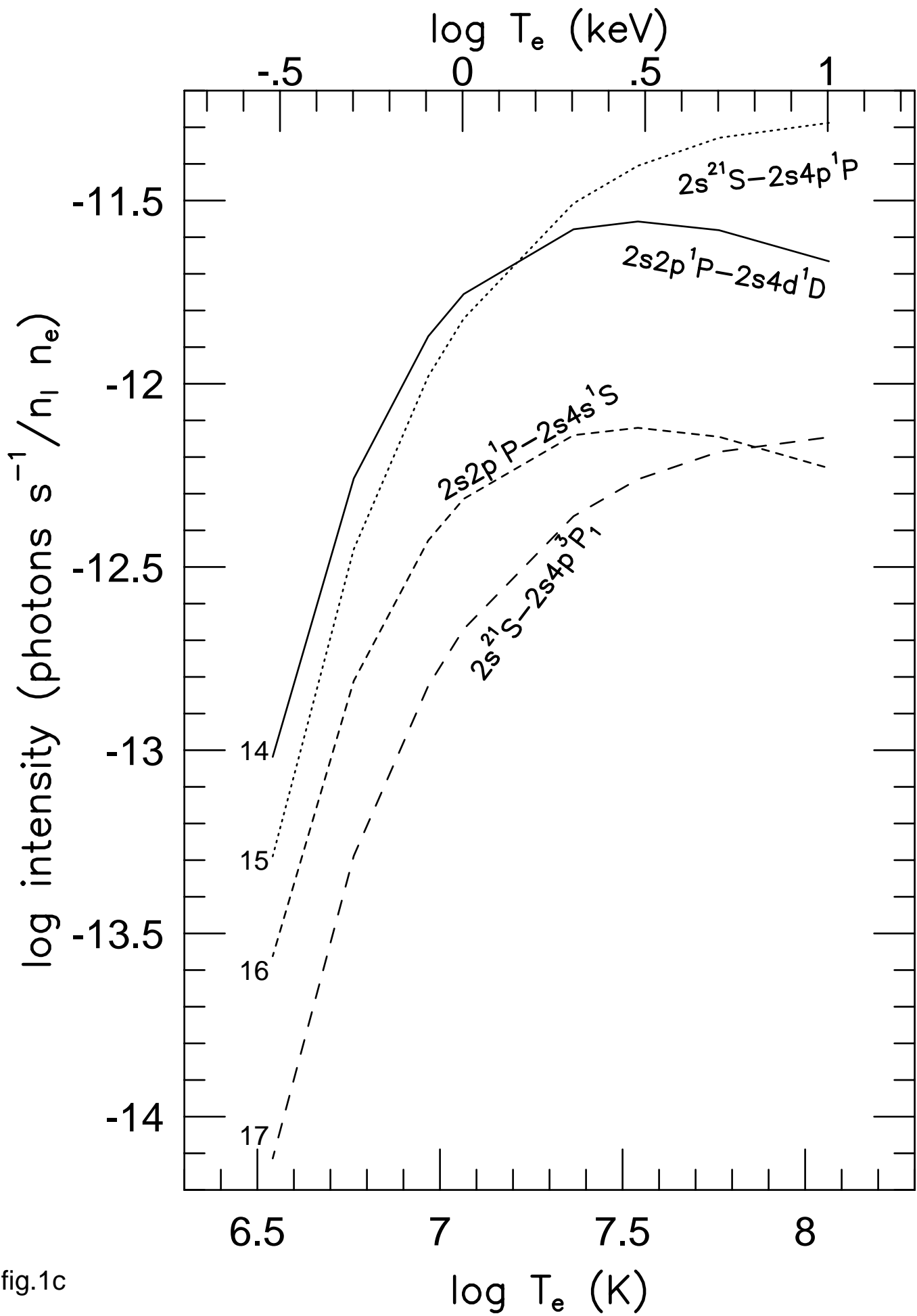


fig.1c

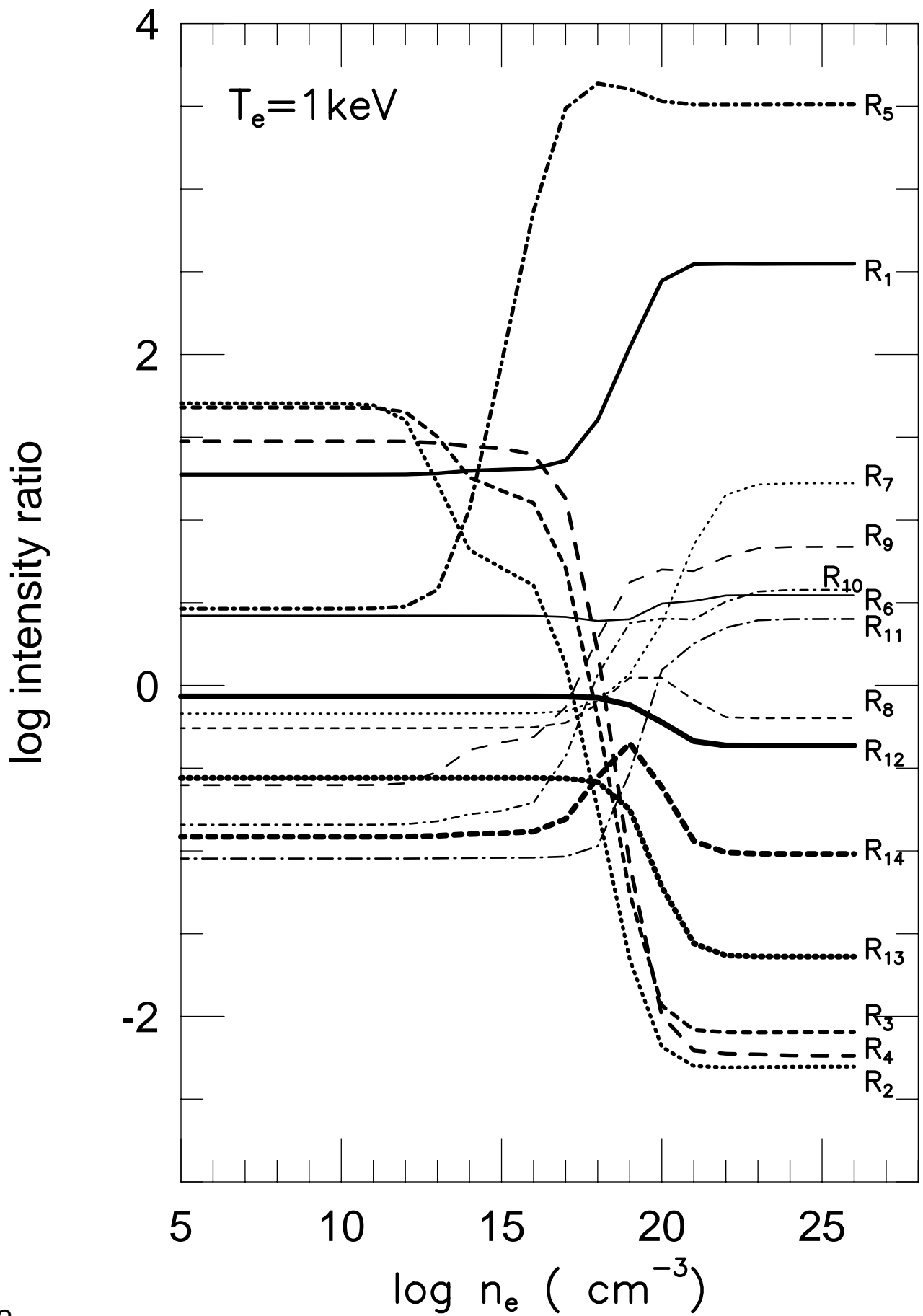


fig.2

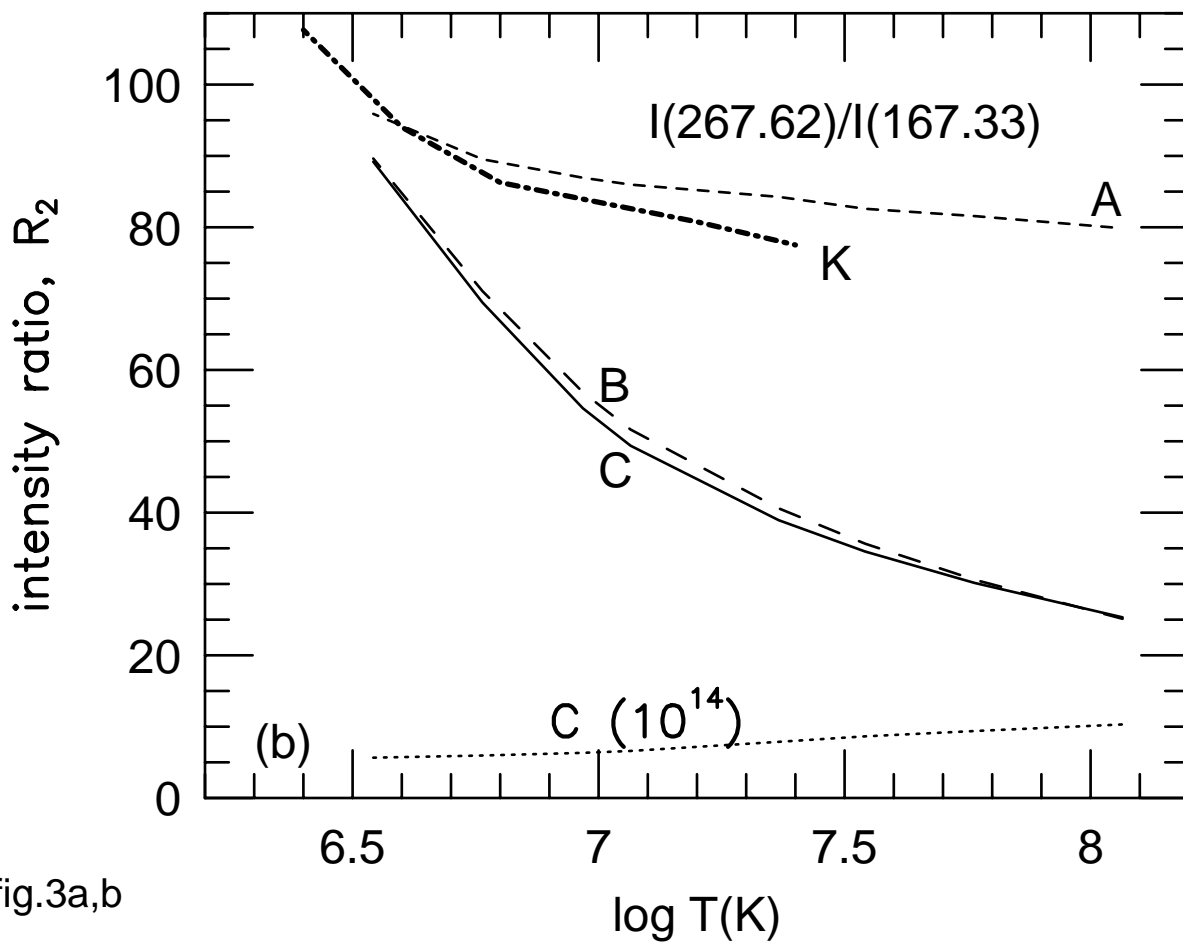
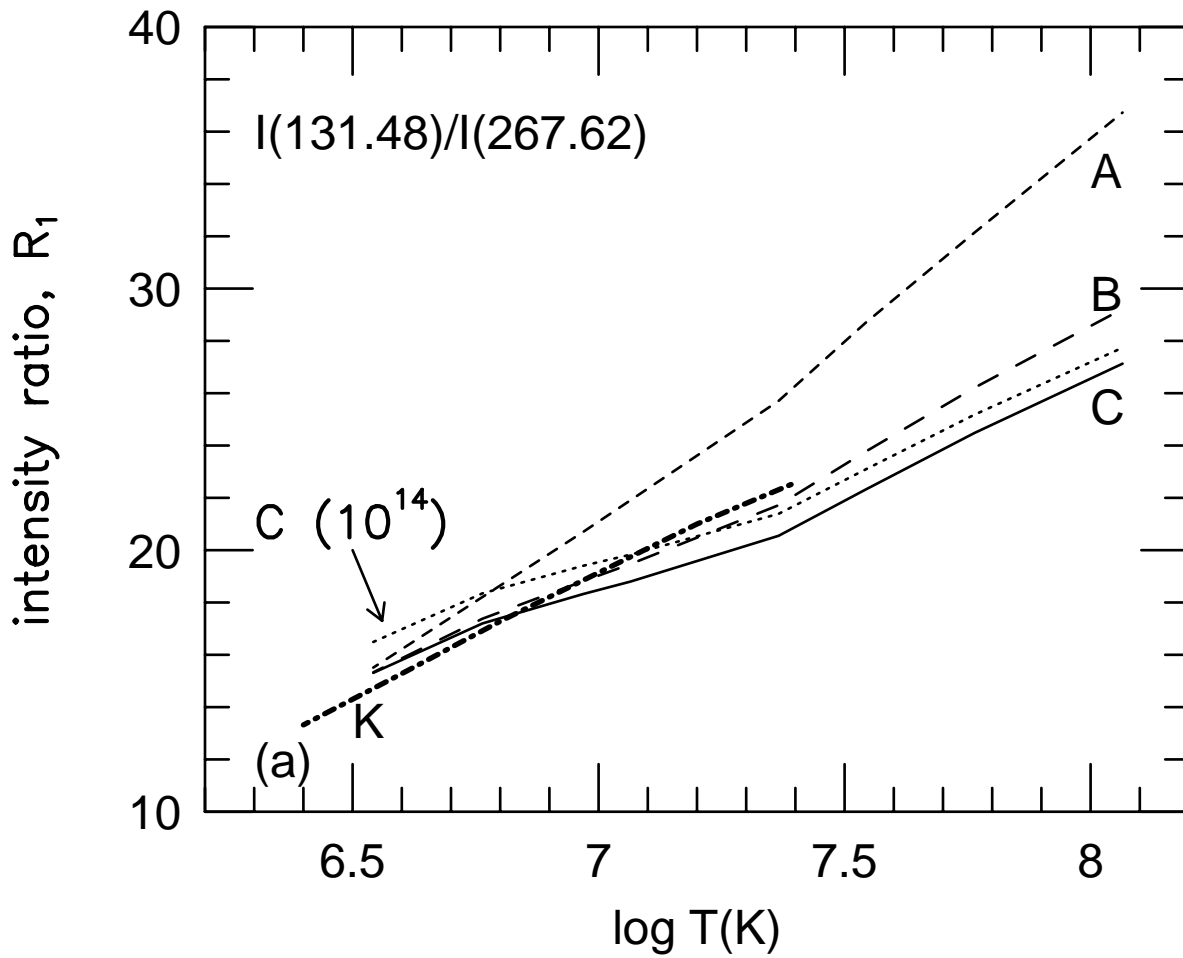


fig.3a,b

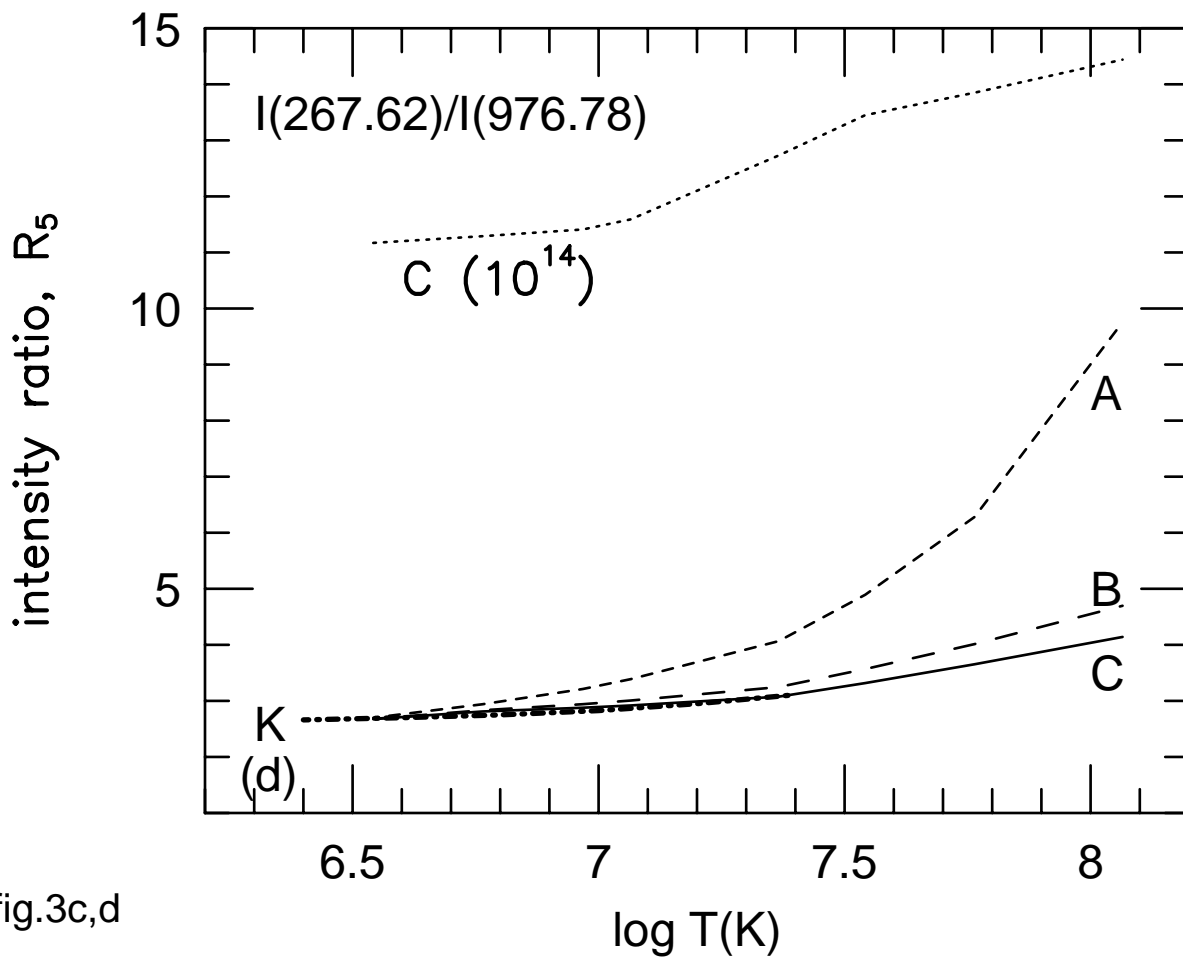
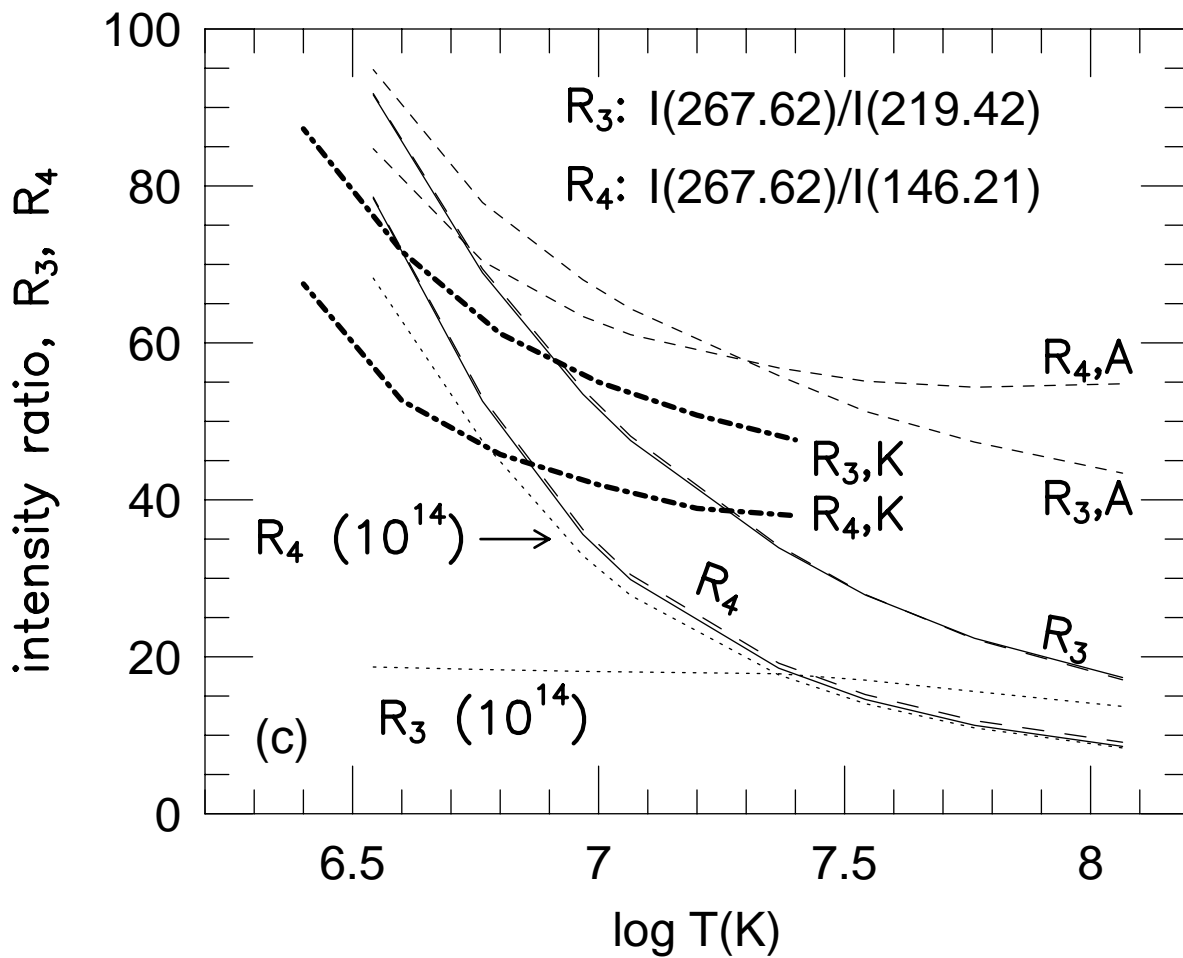


fig.3c,d

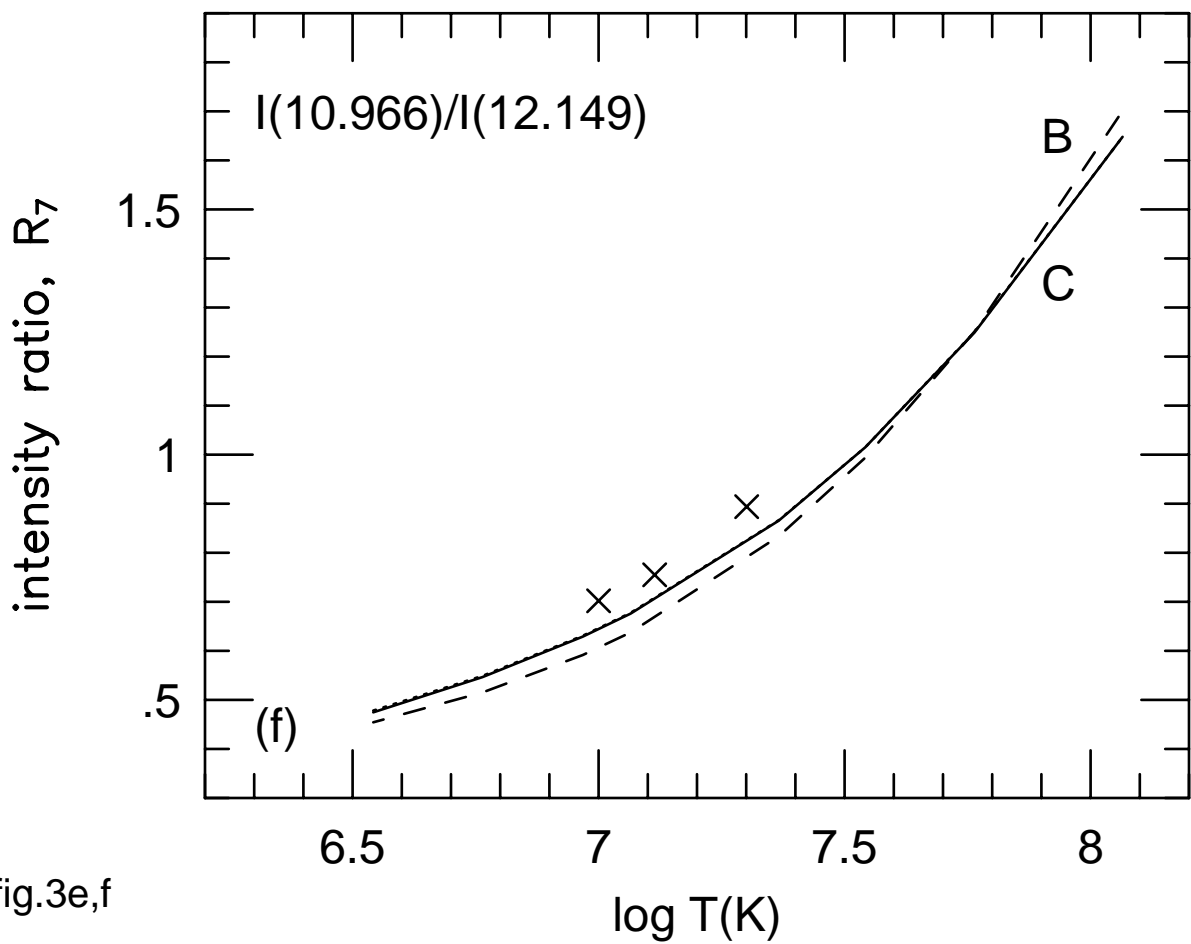
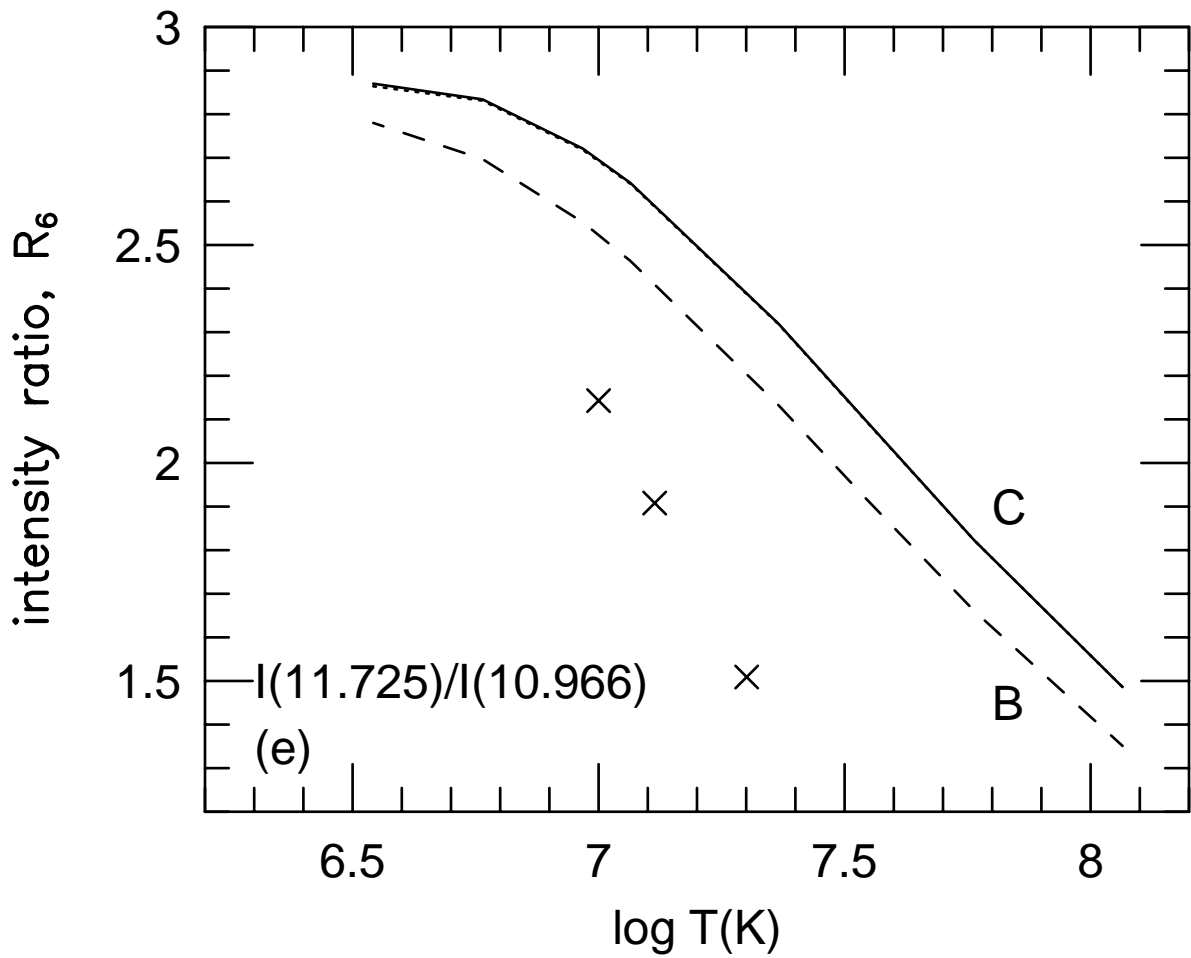


fig.3e,f

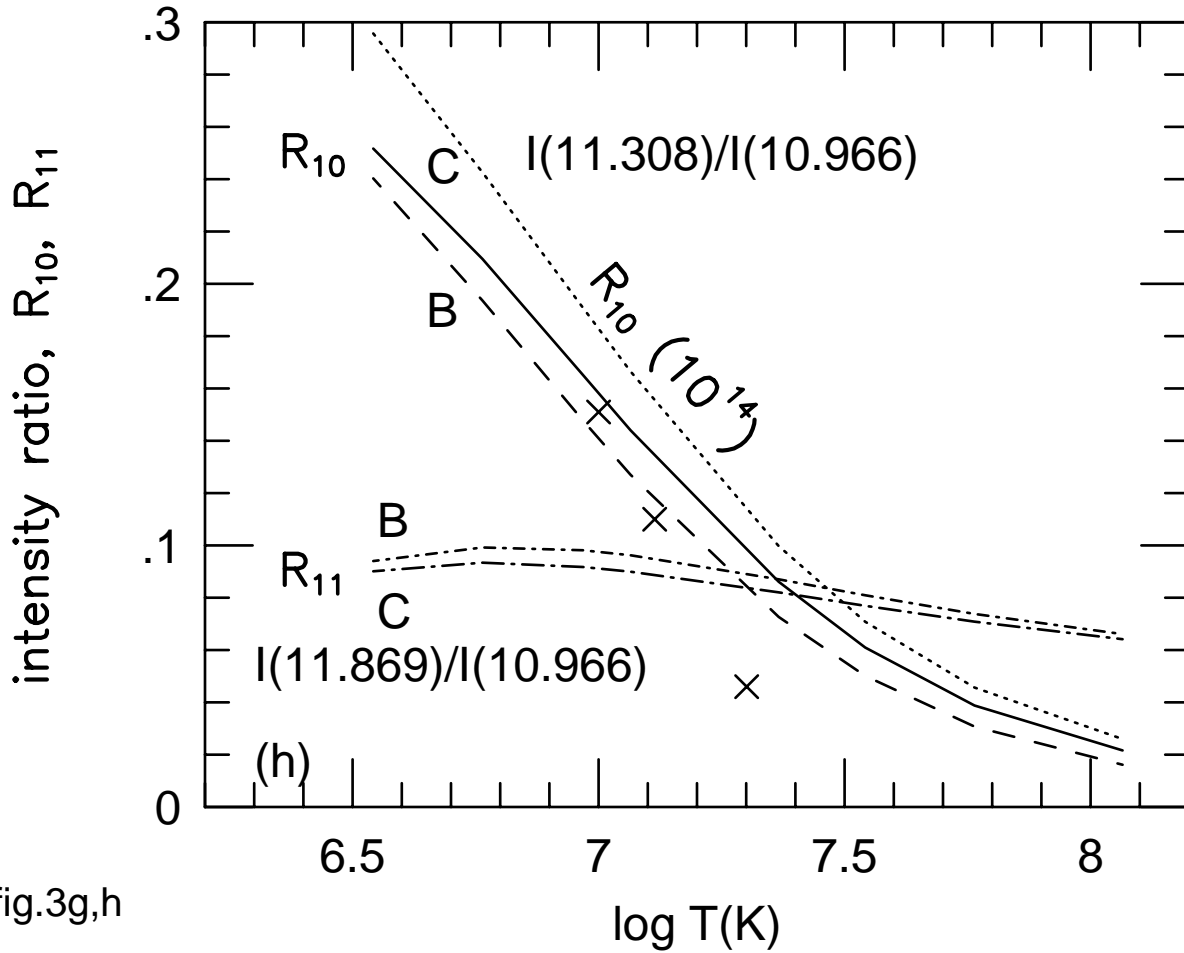
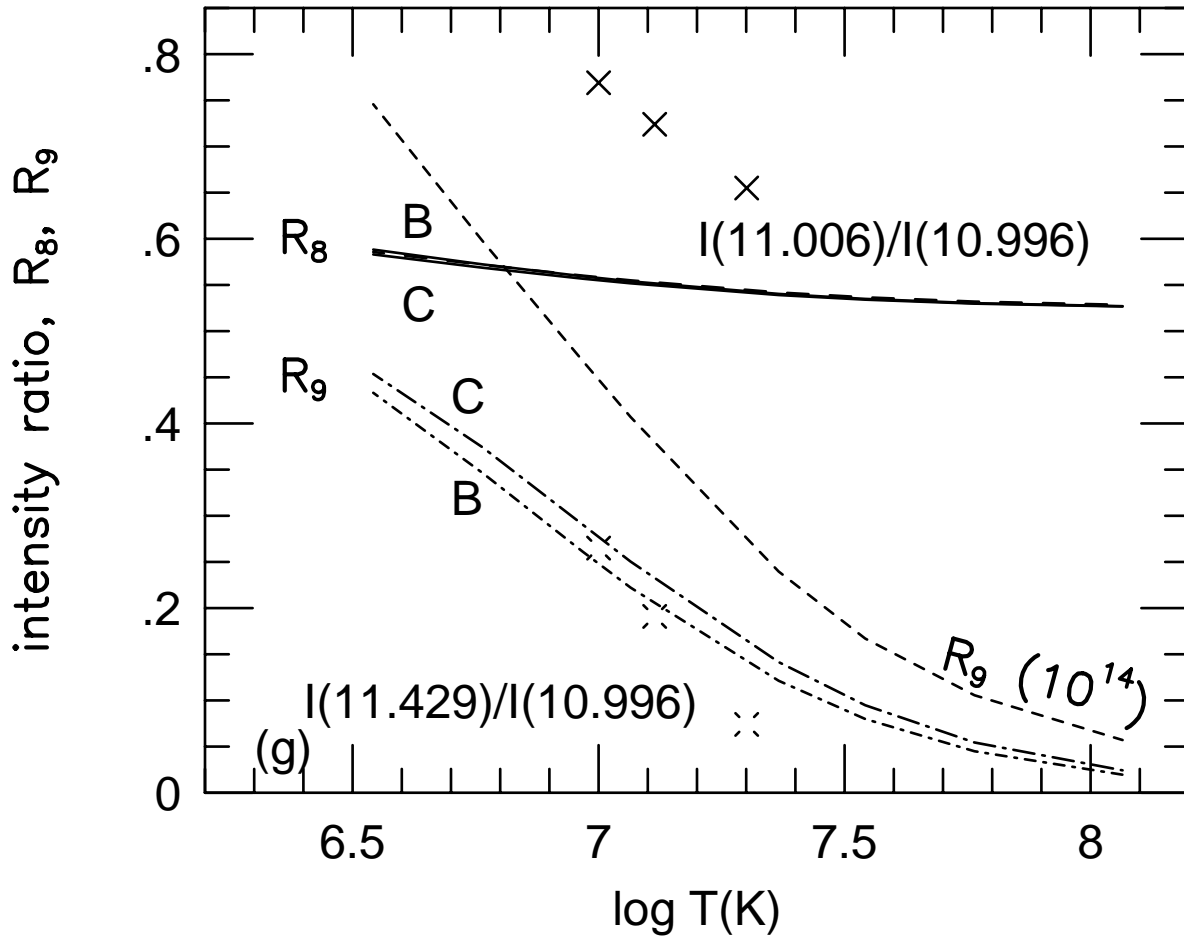


fig.3g,h

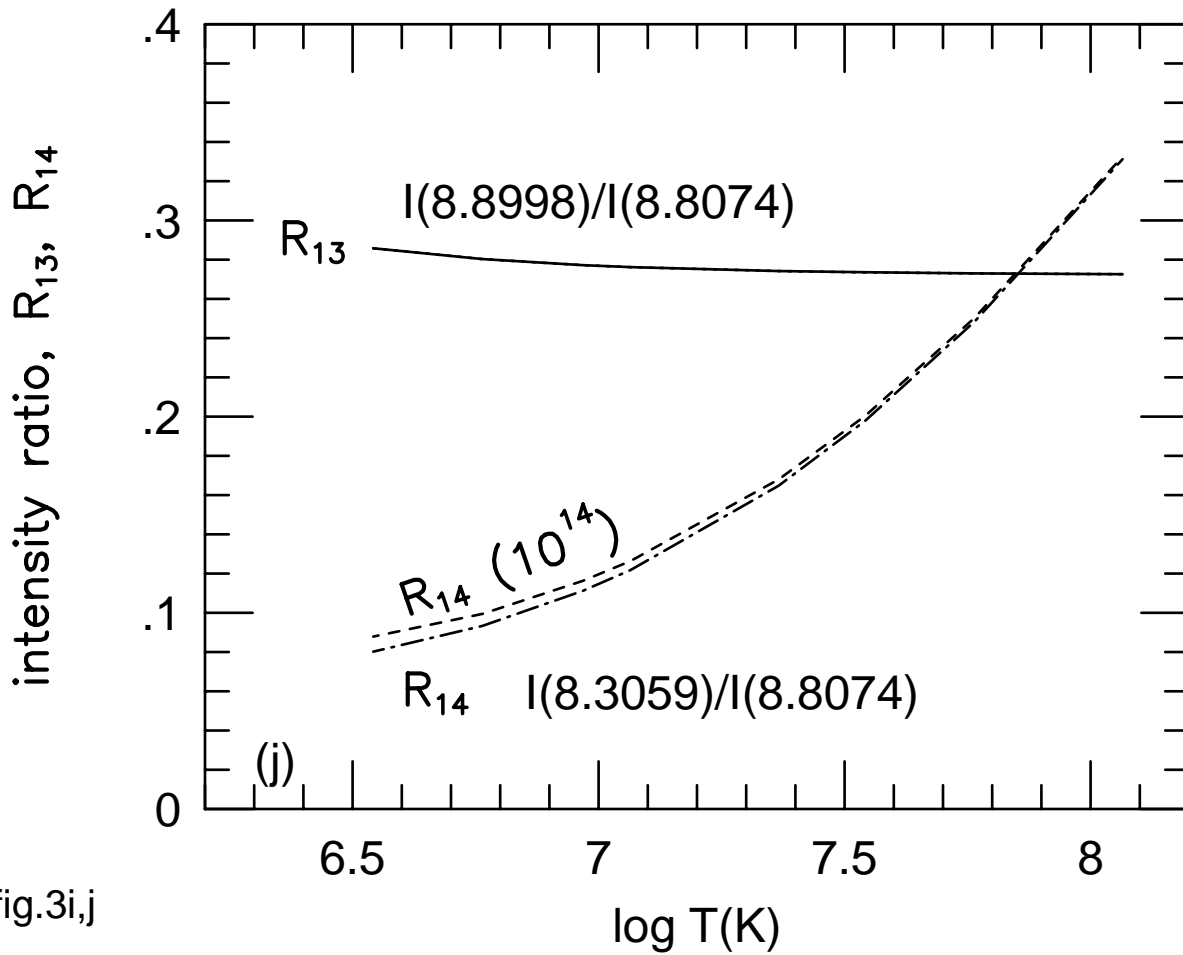
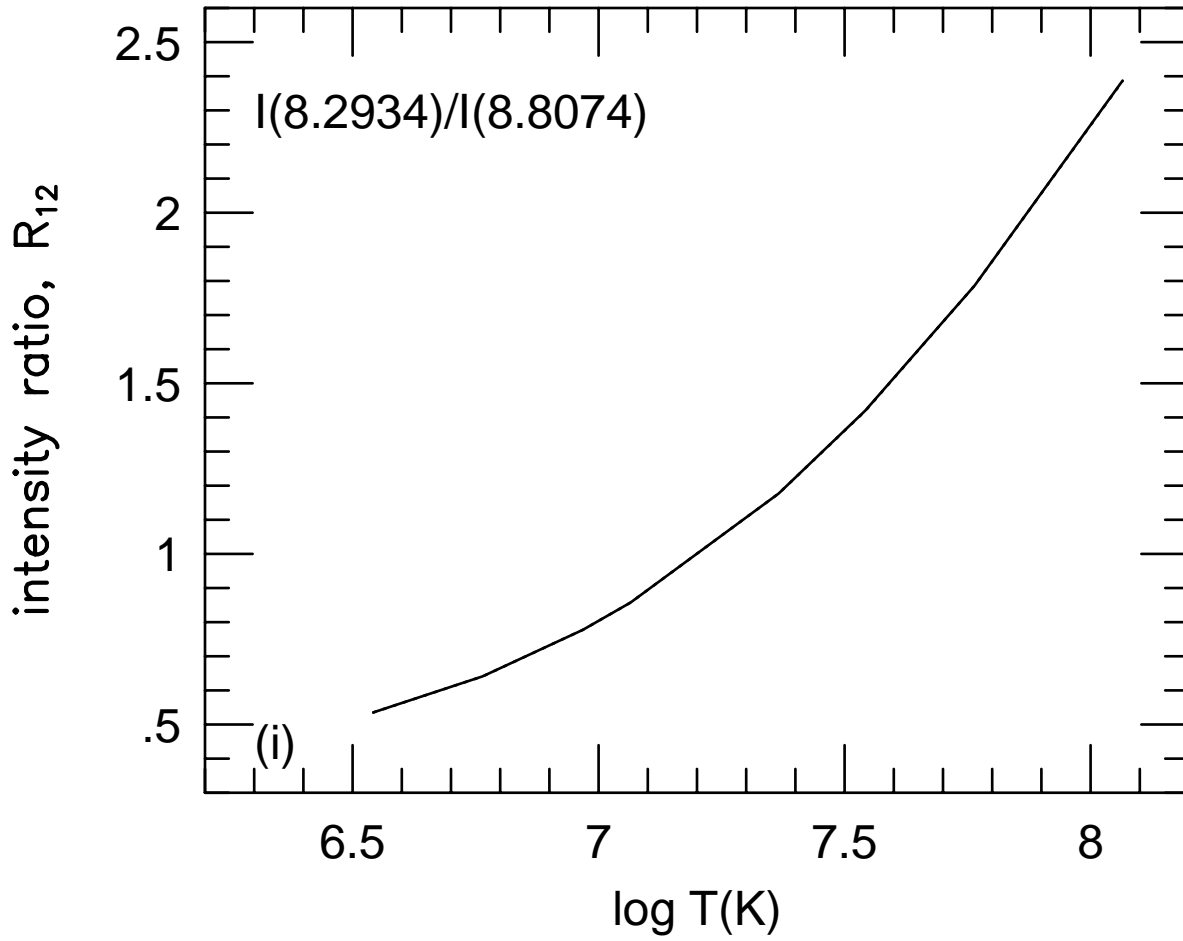


fig.3i,j

fig.4

